Accommodation of Mispair Aligned N^3T-Ethyl-N^3T DNA Interstrand Cross Link†

Mateus Webba da Silva,‡ Christopher J. Wilds,§,|| Anne M. Noronha,§,⊥ O. Michael Colvin,‡ Paul S. Miller,§ and Michael P. Gamcsik*,‡

Department of Medicine, Duke University Medical Center, Durham, North Carolina 27710, and Department of Biochemistry and Molecular Biology, Bloomberg School of Public Health, Johns Hopkins University, 615 North Wolfe Street, Baltimore, Maryland 21205

Received June 29, 2004; Revised Manuscript Received August 4, 2004

ABSTRACT: The solution structure of the undecamer d(CGAAAT*TTTCG)$_2$, where T* represents a N^3T-ethyl-N^3T interstrand cross link, was elucidated using molecular dynamics calculations restrained by NOE and dihedral data obtained from NMR spectroscopy. The ethyl moiety is particularly well-accommodated *between* the minor and major grooves. This is an exceptional example of the plasticity along the axis defined by the stem and a unique finding of an interstrand cross link occupying the area associating minor and major grooves. The mismatch-aligned tethered bases preserve good intrastrand stacking with flanking bases. Base-pair steps adjacent to the lesion site are overwound. Accommodation of the lesion also results in an increase in mispair staggering alignment modulated by flexibility because of the tetrahedral geometry of the exocyclic ethyl carbon atoms. This is mechanically coupled with a small measure of concomitant propeller twisting without an increase in intrastrand base-step distance. Both *x displacement* and sugar puckering are indicative of canonical B DNA throughout the stem. We have thus established that the lesion defined by mismatch-aligned minor groove N^3T-ethyl-N^3T cross-linked thymine bases produces very localized distortions in a DNA stem that may be difficult to recognize by repair mechanisms that are not transcription- or replication-coupled. Thus, this synthetic DNA is a valuable structural probe to study mechanisms of repair.

Many carcinogenic as well as chemotherapeutic agents cause covalent linkages between complementary strands of DNA. Interstrand cross links are highly cytotoxic because they block all processes that require replication and transcription (*1*). There is evidence that these lesions can occur naturally, but they are expected to be rare (*2*). Cross-linking agents are among the most widely used and most effective anticancer agents, as both simple agents or as part of combination therapy regimens. For these drugs, the interstrand cross link is believed to be the critical cytotoxic lesion. In cancer cells, efficient repair of these lesions can lead to drug resistance (*3*). Circumvention of this resistance will require an understanding of the factors involved in their recognition and repair. Both the nature and composition of particular interstrand cross-link repair apparatus are expected to be dependent on the types and extent of distortions to the DNA (*4*). Interstrand cross links can be repaired by human nucleotide excision repair enzymes (e.g., see ref *5*). There are also some indications that the repair of this type of lesion can proceed through the formation of double-strand breaks, which are then repaired by homologous recombination (*6*). However, details are yet to be understood. In this context the use of cross links as structural probes is crucial.

Thymine is photochemically the most reactive base (*7*). It is well-known that exposure to UV induces DNA damage, which is the first step in mutagenesis and a major cause of skin cancer. The *cis-syn* pyrimidine dimer (cyclobutane-type pyrimidine photodimer) is the major photoproduct induced by UV light present in sunlight (*8*) and is one of the principal causes of skin cancer (*9*). This lesion, an intrastrand cross link, has been used extensively as a probe for DNA repair studies. Thymines in different strands of DNA can be targeted by psoralen (*10*). Psoralen intercalates double-stranded DNA and upon absorption of UV light forms a cyclobutane ring with thymidine in one strand. Absorption of a second photon by the monoadduct produces a psoralen cross link. A significant number of studies have been carried out on the repair of psoralen cross-linked DNA, and the structure of the cross link has been determined (*11*−*15*). However, this cross link represents a unique set of structural perturbations and is therefore prone to elicit the assembly of a specific repair apparatus.

Consequently, we are systematically examining the relationship between the nature and extent of alkyl cross-link-induced distortions and their recognition. Essential to this effort has been the development of synthetic strategies to prepare alkyl cross-linked oligonucleotides with defined structure (*16*−*19*). Recently, we reported the synthesis and physical characterization of a series of short DNA duplexes that contain N^3-T-alkyl-N^3T interstrand cross links (*20*). In

† This research was supported by a grant from the National Cancer Institute (CA082785). A.M.N. was supported by a postdoctoral fellowship from the Natural Sciences and Engineering Council (NSERC).

* To whom correspondence should addressed: Duke University Medical Center, Box 2638, MSRB 395, Research Drive, Durham, NC 27710. Phone: (919) 681-2244. Fax: (919) 668-3925. E-mail: michael.gamcsik@duke.edu.

‡ Duke University Medical Center.

§ Johns Hopkins University.

|| Current Address: Department of Chemistry and Biochemistry, Concordia University, Montreal, Quebec, Canada.

⊥ Current Address: Alnylam Pharmaceuticals, Cambridge, MA.

10.1021/bi0486435 CCC: $27.50
Published on Web 09/08/2004

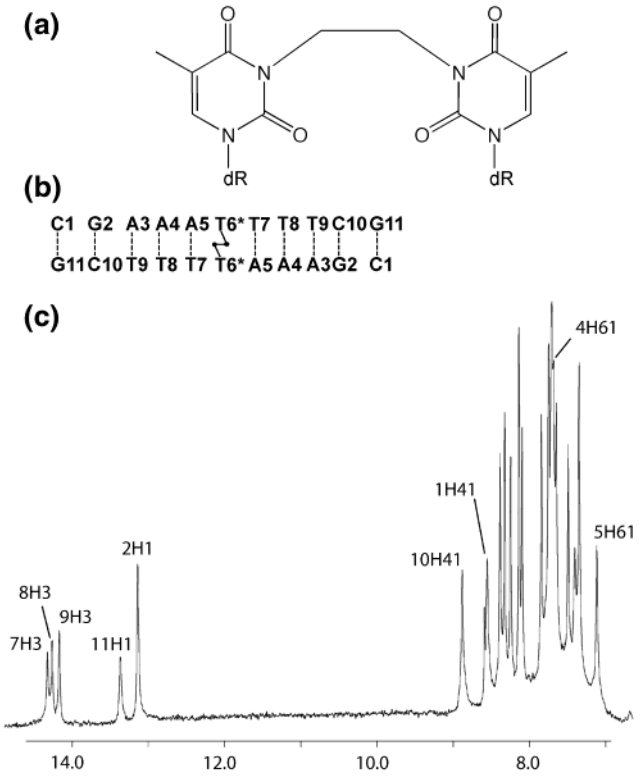

FIGURE 1: (a) Scheme of self-complementary duplex d(CGAAAT*TTTCG)$_2$. The dotted lines indicate hydrogen bonds, and the filled line indicates the interstrand cross link. (b) Chemical structure of cross-linked cytosines. (c) One-dimensional ^{1}H NMR spectrum of d(CGAAAT*TTTCG)$_2$ in ^1H_2O solution containing 0.1 M NaCl at pH 7.4 showing assigned imino proton signals. The imino of G11 is broad because of the increased water accessibility to this terminal residue.

the current paper, we describe the structural properties underpinning the differences in the immediate environment of a N^{3}T-ethyl-N^{3}T interstrand cross link (hereafter denoted T*, Figure 1a) that has been inserted into a scaffold in which the cross link is mispair-aligned, i.e., 5′-CGAAAT*TTTCG-3′ (Figure 1b). Comparisons of the structure of this oligomer with that of N^{4}C-ethyl-N^{4}C (hereafter denoted C*) in the same scaffold, 5′-CGAAAC*TTTCG-3′ (*21*), reveal significant structural features that will enrich the available structural probes for mechanistic DNA repair studies.

MATERIALS AND METHODS

The oligomer d(CGAAAT*TTTCG)$_2$ was synthesized and purified using methods previously described to prepare short DNA duplexes that contain an N^{3}T-alkyl-N^{3}T interstrand cross link (*20*). The duplex gave the expected nucleoside−cross-link ratios when digested with a combination of snake venom phosphodiesterase and calf intestinal alkaline phosphatase, followed by analysis by reversed-phase HPLC. The mass of the duplex was consistent with its structure as analyzed by mass spectrometry (*m*/*z*: calcd, 6687.2; found, 6691.0). The NMR sample was prepared by dissolving the molecule in 0.25 mL of buffer containing 15 mM sodium phosphate (pH 7.4) and 100 mM NaCl resulting in a solution approximately 3 mM in single-strand concentration.

NMR Spectroscopy. Standard NMR experiments were recorded on Varian Inova 500, 600, and 800 MHz spectrometers. We recorded NOESY[1] (200 and 60 ms) spectra in ^1H_2O at 0 °C and NOESY (*22*) (50, 100, 150, 200, and 250 ms), DQF−COSY (*23*), TOCSY (*24*) (spin-lock time of 40 ms) in ^2H_2O at 20 °C. In ^1H_2O, data were acquired with a jump-and-return pulse sequence (*25*) and in ^2H_2O, with Watergate suppression of the residual water signal (*26*). All data sets were acquired in a phase-sensitive mode (TPPI). In ^1H_2O, NOESY data sets were collected with 8 k complex points over a spectral width of 16 kHz with 300 t_1 increments. In ^2H_2O, NOESY data sets were collected with 3412 complex points and 300 t_1 free induction decays covering a spectral width of 8 kHz. TOCSY spectra were recorded with 3798 t_2 complex points and 256 t_1 increments, and the DQF−COSY was acquired with 3468 t_2 complex points over 512 t_1 increments. Proton chemical shifts were referenced to internal sodium 2,2-dimethyl-2-silapentane-5-sulfonate (DSS). All data sets were processed using VNMR (Varian Instruments) and FELIX 2000 (Accelrys Inc.). Structures were visualized and figures prepared from Insight II (Accelrys Inc.).

Distance and Torsion Restraints. NOE cross peaks involving exchangeable protons in NOESY spectra (50 and 200 ms mixing times) in H_2O buffer were classified as strong (strong intensity at 60 ms), medium (barely observable at 60 ms), and weak (not observable at 60 ms and observable at 200 ms), and the observable proton pairs were restrained to distances of 3.0 ± 0.6, 4.0 ± 1.0, and 5.0 ± 1.2 Å, respectively. NOE buildups for nonexchangeable protons were derived from NOESY spectra in ^2H_2O buffer recorded as a function of the mixing time (50, 100, 150, 200, 250 ms). Distances were estimated from the initial buildup rates within FELIX 2000 (Accelrys). The cytosine H5−H6 interproton distance of 2.46 Å was used as a reference. The upper and lower bounds were allowed to vary ±30%. Overlapping cross peaks were given generous bounds (up to ±80%). Atoms participating in experimentally identified canonical base pairing (based on NOE patterns) were restrained with distances corresponding to ideal hydrogen-bond geometry (*27*) between donor and acceptor atoms.

The appearance of strong H1′−H2″ and very weak to no H2″−H3′ cross peaks in the DQF−COSY spectrum indicates that the most populated conformations are S type. Thus, δ and the endocyclic $\nu(0)-\nu(4)$ torsion angles were moderately constrained, leaving the sugar free to take any conformation without an energy penalty between C4′-*endo* and O1′-*endo*, including C2′-*endo*. CURVES 5.2 (*28*) was used to estimate DNA conformation and helical parameters.

Distance-Restrained Molecular Dynamics Regularization. Calculations were performed with XPLOR (*29*) using the CHARMm force field (*30*) and adapted for restrained molecular dynamics (rMD) for nucleic acids. All calculations were executed in vacuo without explicit counterions. The cross link was placed in the major groove as defined by the available NMR restraints. The initial distance geometry and simulated annealing refinement protocol started from 250 different structures generated from sets of two strands, each 11 nucleotides long, randomized over all dihedral angles. A number of structures (36 of 250) emerged separated from

[1] Abbreviations: COSY, 2D-correlated spectroscopy; DQF−COSY, double-quantum-filtered COSY; DSS, 2,2-dimethyl-2-silapentane-5-sulfonate; NOE, nuclear Overhauser effect; NOESY, 2D NOE spectroscopy; rMD, restrained molecular dynamics; TOCSY, 2D total correlated spectroscopy.

nonconverged structures by large gaps in all components of the potential energy function (dihedral angles, van der Waals, NOE violations, and covalent geometry). This set was subsequently submitted for further refinement. Sets of rMD calculations were performed using random velocities fitting a Maxwell−Boltzmann distribution. The empirical energy function was developed for nucleic acids and treated all hydrogens explicitly. It consisted of energy terms for hydrogen bonding and nonbonded interactions, bonds, bond angles, torsion angles, and tetrahedral and planar geometry, including van der Waals and electrostatic forces. The effective function included terms describing distance and dihedral restraints, which were in the form of square well potentials (*31*). Most estimated distances from NOE data analysis were incorporated as ambiguous restraints using the "SUM averaging" option of XPLOR, because they could reflect intra- and/or interstrand contributions. On the basis of the 2-fold symmetry, noncrystallographic symmetry restraints were imposed on all atoms. Planarity restraints were used in all stages of computations. The simulated annealing procedure consisted of a total of 53 ps of rMD including 7 ps of heating from 300 to 1000 K, 20 ps of scale-up of restraints at high temperature, 14 ps of cooling to 300 K, and 12 ps of equilibration rMD. The temperature was controlled by coupling the molecules to a temperature bath with a coupling constant of 0.025 ps (*32*). The van der Waals term was approximated using the Lennard−Jones potential energy function, and bond lengths involving hydrogens were fixed with the SHAKE algorithm (*33*), during molecular dynamics calculations. Coordinates (accession number 1S37) have been deposited in the PDB data bank.

RESULTS

Sharp peaks for three lower field thymine imino and two guanine imino peaks are observable in the one-dimensional region between 13.0 and 14.5 ppm, and sharp and well-resolved peaks are observable in the aromatic proton spectrum (Figure 1c), indicating a stable structure suitable for NMR studies. The number of peaks corresponds to one conformer with complementary base pairing.

Resonance Assignments. Assignment of the imino and amino exchangeable protons was performed following analysis of 1−1 NOESY spectra at 60 and 200 ms mixing times (0 °C) and based on assignments of the nonexchangeable region. Shown in Figure 2a is a selected region of a 1−1 NOESY spectrum (200 ms) depicting selected assignments for exchangeable protons. NOEs between thymine imino protons and adenine H2 and amino protons across A/T base pairs and between guanine imino and cytosine amino and H5 protons across G/C base pairs are observed. Interstrand dipolar connectivities such as those for A3 (T9H3−A3H61, T9H3−A3H62, and T9H3−A3H2), A4 (T8H3−A4H61, T8H3−A4H62, and T8H3−A4H2), A5 (T7H3−A5H61, T7H3−A5H62, and T7H3−A5H2), C1 (G11H1−C1H42 and G11H1−C1H41, not shown), and C10 (G2H1−C10H42 and G2H1−C10H41, not shown) suggest Watson−Crick base-pairing throughout the stem. Observation of cross-strand peaks T8H3−A5H2, T9H3−A4H2, and intrastrand G2H1−A3H2 indicate typical B-DNA base-step and axis-displacement environments for the three-adenine segment. The broadness of the G11H1 imino proton resonance of this terminal base (Figures 1c and 2a) might be the result of increased accessibility of water to the hydrogen bonds forming the terminal base-pair C1/G11.

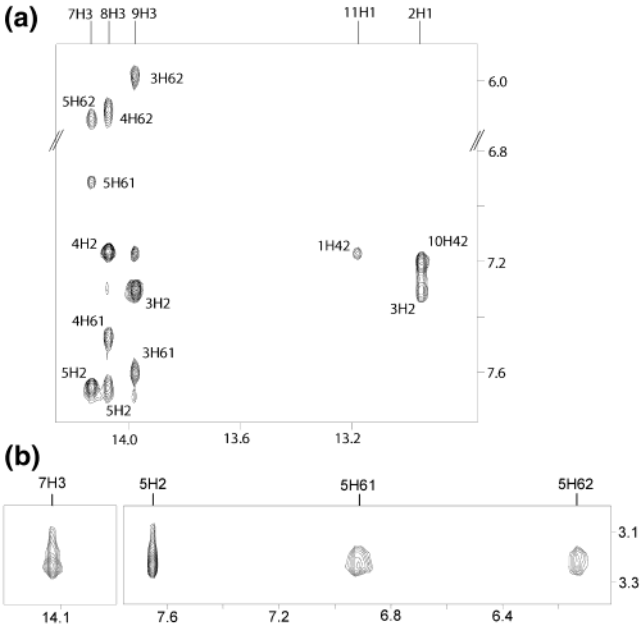

FIGURE 2: Selected spectral regions from a NOESY (200 ms) in ^1H_2O at 0 °C and pH 7.4 and 0.1 M NaCl. (a) Assignments indicated have relevance in establishing canonical base pairing and in (b) a spectral region depicting assignments for the alkylated base, T*6.

The environment of the alkylated base within the DNA stem is well-characterized through a good number of dipolar connectivities. Figure 2b depicts some of the connectivities of the cross-linking ethyl moiety. The portions of the spectrum at 0 °C show contacts to the N + 1 flanking base T7H3. This is only possible if a proton bound to an sp3 carbon is not in the same plane as C(aromatic)−N3−C(aromatic). Contacts of the exocyclic methylene protons to the major groove oriented amino of intra- or interstrand adenine A5 (5H61 and 5H62) positions and adenine 5H2 (also intra- or interstrand) place the ethyl moiety *between* minor and major groove.

Assignments of the protons were made through analysis of standard NOESY, TOCSY, and DQF−COSY spectra by established methods (*34*, *35*). Assignments of the H8/H6/H5 base and H1′ sugar protons (Figure 3) were made through analysis of the 50 and 250 ms NOESY spectra. At 250 ms mixing time, we can readily trace the sequential dipolar connectivities between the base and its own 5′-flanking sugar H1′ protons along individual strands as expected for right-handed DNA. These were further substantiated by sequential analysis in H6/H8−H3′ by aromatic−aromatic cross peaks and H6/H8−H2′/H2″ connectivities. At low mixing time (50 ms), weak H8/H6−H1′ cross peaks were observed indicating that all residues are anti (when compared to C1H6−C1H5 and C11H6−C11H5). Still in Figure 3 typical B-DNA cross strand (*i*)AH2−(*j* + 1)NH1′ (*i* and *j* represent different strands, and N is any base; A4H2−T9H1′, A5H2−T8H1′, and A3H2−C10H1′), intrastrand (*i*)AH2−(*i* + 1)NH1′ (A4H2−A5H1′, A5H2−T6H1′, and A3H2−A3H1′), and intraresidue (A4H2−A4H1′, A5H2−A5H1′, and A3H2−A3H1′) are also observable. The stereospecific assignment of individual H2′ and H2″ protons was derived from comparison of intensity of the H1′−H2′ and H1′−H2″ intraresidue cross peaks in a 50 ms NOESY spectrum. At

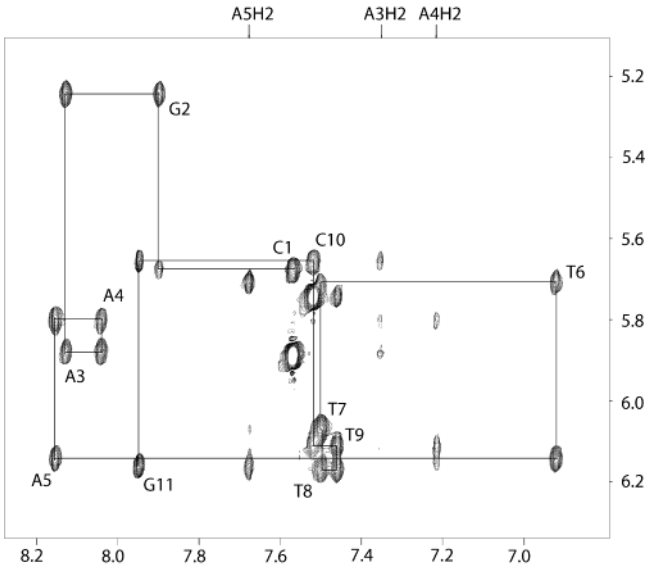

FIGURE 3: Selected region of NOESY spectrum (250 ms) of (a) d(CGAAAT*TTTCG)$_2$ in ^2H_2O solution at pH 7.4 and 20 °C and 0.1 M NaCl showing NOE correlations between H8/H6/H2/H5 and H1′. The self-peaks involving H1′ protons have been labeled, and their sequential connectivities have been drawn.

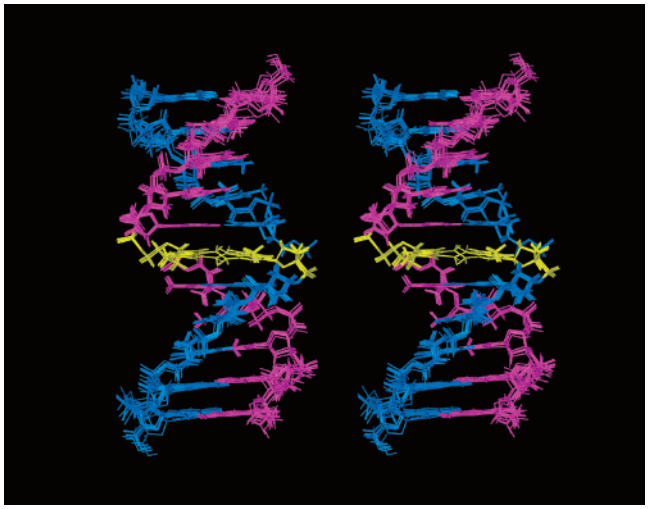

FIGURE 4: Stereoview of a superposition of eight lowest energy refined structures of the duplex d(CGAAAT*TTTCG)$_2$. The individual strands are colored pink and blue, and the cross link is colored yellow.

this mixing time, the intraresidue H1′−H2′ cross peaks are stronger than H1′−H2″ in B DNA. DQF−COSY spectral patterns indicated that H1′−H2′ coupling constants were reasonably large (>6 Hz), with only one terminal residue (G11) showing strong H2″−H3′ cross peaks. This sugar pucker was left unrestrained during structure calculations. In contrast to all other nucleotides, the chemical shift of G11H2′ also appears at a higher field to G11H2″. Therefore, the sugar geometries are predominantly S type (*36*), and consequently the strand structures may be considered to belong to the B-DNA family.

Structural Features. A stereoview of eight superpositioned refined structures of the duplex d(CGAAAT*TTTCG)$_2$ is plotted in Figure 4 and exhibits average heavy-atom root-mean-square deviations (rmsd's) to the mean structure of 0.5 ± 0.2 Å. The input and structure convergence parameters are listed in Table 1. The structure of the right-handed self-

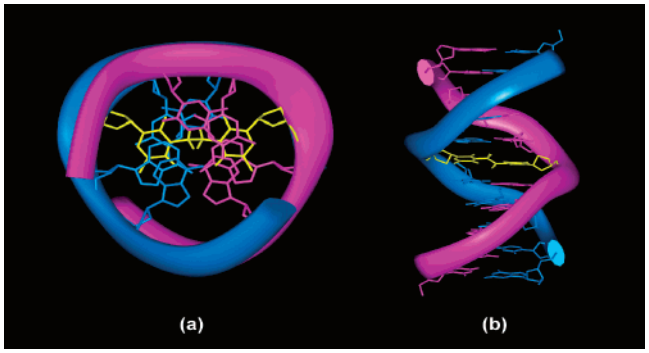

FIGURE 5: Orthogonal views of the duplex structure of d(CGAAAT*TTTCG)$_2$. The individual strands are colored pink and blue, and the cross link is colored yellow. (a) View into the stem axis showing the alignment of the mispair aligned basis with the ethyl moiety between the major and minor grooves and stacking interactions for the nearest-neighbor bases to the lesion. (b) View orthonormal to a, depicting the length of the stem and the regularity of the backbone.

Table 1: Restraints and Refinement Statistics for Eight Selected Structures for d(CGAAAT*TTTCG)$_2$

NMR restraints	
total number of restraints	343
nonexchangeable protons	213
exchangeable protons	22
hydrogen bond restraints (empirical)	48
dihedral angle restraints (pucker only)	50
noncrystallographic symmetry restraints on all heavy atoms	
structural statistics	
NMR *R* factor ($R_{1/6}$)	0.104−0.105
NOE rmsd (Å) total	0.032−0.035
NOE violations exceeding 0.2 Å	0
heavy-atoms pairwise rmsd	0.5 ± 0.2

Table 2: Geometrical Parameters for the Lowest Energy Structure of d(CGAAAT*TTTCG)

base pair	(C1′−C1′) (Å)	stagger[a] (Å)	buckle[a] (deg)	propeller[a] (deg)
G2−C10	10.9	0.0	0.0	0.6
A3−T9	10.4	0.1	0.4	1.7
A4−T8	10.9	0.2	1.4	2.2
A5−T7	10.5	0.0	2.2	2.5
T6*−T6*	10.4	0.7	0.0	19.7

[a] Absolute magnitude.

complementary duplex with antiparallel strands is well-defined in the internal segments encompassing the cross-linked nucleotides up to the end residues (G11 and C1), where fraying is apparent. Progression along the backbone presents little departure from uniformity, showing somewhat lesser regularity in the lesion moiety (parts a and b of Figure 5). The compactness of the stem is barely affected as seen from the regularity of the disposition of the bases in the interior of the helix, and the hydrogen bonding for the Watson−Crick base pairing has not been disrupted. In Figure 5b the cross link (in yellow) accommodates itself well *between* the minor and major grooves. This unique feature is only possible because of two concomitant effects apparent from inspection of the geometrical parameters as shown in Table 2. The T6*−T6* mispair experiences propeller twisting 1 order of magnitude greater than for the rest of the base pairs in the stem. This effect diminishes progressively away from the lesion. This feature is further demonstrated by the fact that simultaneous to the large magnitude of propeller

twisting between the cross-linked bases is the lack of buckling. However, for the adjacent bases, A5−T7, some buckling is observed and its measure diminishes progressively away from the lesion. In standard B DNA, the intrastrand base stacking is coupled with a stepwise twisting of 36° for every canonical base pair. This structure results in a stem mean magnitude for intrastrand interbase twist of 38° for the undecamer. The base steps A4pA5 and T7pT8 are dramatically overwound (by 43°). Notwithstanding, from Figure 5a, it is apparent that there is good intrastrand base stacking throughout the stem. Nonstandard backbone torsion angles are observed for some residues (see Table S2 in the Supporting Information). Particularly, the dihedral angles α,*t* and β,g^+ for A5, as well as α,g^+ and ϵ,g^- for A3. They reflect the extent of the accommodation to trends in the collective mechanics in the DNA backbone resultant from the lesion. The sugar puckers for these two residues, as with the others, populate preferentially sugar puckers of the S type, albeit deviating from C2′-*endo* (Table S1 in the Supporting Information). In summary, noticeable distortions because of the cross link are illustrated in the magnitudes of intrabase-pair staggering, buckle, and propeller twist but not in cross-strand (C1′−C1′) distances and *x displacement* (not shown in the table). The latter, coupled with sugar puckers populating predominantly S-type conformations, and torsion angles along the sugar phosphate backbone populating predominantly the B_I conformation result in an overall canonical B-DNA topology.

DISCUSSION

We have solved the first solution structure of an interstrand covalent cross link between two thymines alkylated at the N3 positions. The structure shows that the ethyl cross link can be accommodated between the complementary DNA strands with little distortion. The experimental observation of typical NOE restraints for Watson−Crick base pairing for all canonical base pairs allowed us to conclude that there were no hydrogen-bond disruptions. Most interestingly, the cross link was accommodated along the region between the major and minor grooves. Notably, because of the fact that the exocyclic cross-linking ethyl moiety was bound to the aromatic rings at the N3 position, the orientation of the base in respect to the stem did not deviate from its normal position; i.e., the base maintains the same base-stacking pattern as compared to a noncross-linked base-paired thymine. This is an interesting example of the considerable DNA plasticity along the axis defined by the stem. Furthermore, we observe flexible exocyclic ethyl moieties as observed for the eight lowest energy structures selected (Figure 4).

It is interesting to compare the three-dimensional structures bearing an ethyl moiety in T*−T* with our earlier study of the same scaffold containing a C*−C*. In the structure of the mispair aligned C*−C* (*21*), the ethyl cross link bridges the exocyclic amino and therefore its disposition results in the major groove. This feature is also observed for the same lesion in a C*pG step within the same scaffold (unpublished results). In contrast to T*−T*, in C*−C*, we observed features that represent a departure from canonical B DNA toward A DNA (in sugar puckering and *x*-axis displacement), introduced by the lesion. The differences seem mostly to be a reflection of the interplay between two different effects: the magnitudes of staggering and propeller twisting between the mispair-aligned bases. Staggering is less pronounced in C*−C* because the ethyl moiety connects the bases through major-grove-pointing exocyclic nitrogen atoms and therefore induces greater deviation from base-pair planarity than displacement from the plane axis. In contrast, the T*−T* lesion has the cross-link bound to the base at the N3 position, i.e., between its minor groove edge and Watson−Crick edge. Therefore, accommodation of the lesion results in a greater displacement from the plane of the base mispair alignment mostly because of the tetrahedral arrangement on the sp3 ethyl carbon atoms. This is achieved with a small measure of concomitant propeller twisting.

Even though our understanding of the molecular basis of DNA repair has markedly increased in the past decade, the main DNA repair pathways in humans, direct repair, base-excision repair, nucleotide-excision repair, mismatch repair, homologous recombination, and nonhomologous end joining, are still not thoroughly understood in structural mechanistic detail. This is particularly true in the case of the repair of alkyl interstrand cross links. The efficiency and mechanism of damage repair is likely to depend on the extent to which the lesion alters the structure of DNA, hence making it recognizable for the repair proteins involved. To gain a better understanding of the role of lesion-induced perturbations on DNA repair, we are developing well-characterized probes to study mechanisms of repair of major-groove-aligned DNA alkyl interstrand cross links. Thus, the N^4C-alkyl-N^4C interstrand cross link when inserted into the scaffold 5′-CGAAAC*TTTCG-3′ can induce distinct structural alterations including disruption of the base pairing, unwinding of the double helix, bending of the DNA toroid, and backbone flexibility (*21*). In contrast, the present study shows that the N^3T-ethyl-N^3T cross link does not cause significant changes in the major or minor grooves and does not induce changes in the sugar puckers beyond canonical B-DNA plasticity. However, we can expect changes in the rates of sugar pucker dynamics, deviations from canonical backbone angles, and changes in the partitioning of cations into the minor groove because of the hydrophobic character of the cross-linking moiety. These factors could provide a basis for damage recognition by cellular repair proteins. Alternatively, because the N^3T-ethyl-N^3T cross link induces minimal structural perturbation, lesion recognition may be dependent upon DNA transcription or replication. Experiments are currently in progress to examine the repair of DNA that contains N^3C-alkyl-N^3C and N^3T-alkyl-N^3T interstrand cross links.

Novel cross-linking agents continue to be produced in an attempt to generate more selective and less toxic treatments (*37*). These include molecules that are selective for an interaction with DNA, produce a greater yield of interstrand cross links than other DNA lesions, are more selective for particular sequences of DNA, and are bioreductive agents with the potential to produce cross links selectively in hypoxic regions of tumors. One of the greater limitations still is the fact that cross links produced are readily repaired in many types of tumor cells. To address some of these issues, a new generation of highly active sequence-specific DNA minor groove cross-linking agents are being rationally designed (*38*). They produce lesions that cause minimal distortions to the normal DNA structure and, as a result, seem to evade the recognition and repair mechanisms used for the

processing of the more distorting cross links produced in the major groove by conventional cross-linking drugs. These new drugs may have an important clinical role in the future treatment of cancer.

ACKNOWLEDGMENT

Duke University NMR Center was established with grants from the NIH, NSF, and the North Carolina Biotechnology Center.

SUPPORTING INFORMATION AVAILABLE

Tables with geometrical parameters and backbone torsion angles for the lowest energy calculated structure as well as one figure showing a DQF−COSY spectrum of d(CGAAA-T*TTTCG)$_2$ at 20 °C. This material is available free of charge via the Internet at http://pubs.acs.org.

REFERENCES

1. Dronkert, M. L., and Kanaar, R. (2001) Repair of DNA interstrand cross-links, *Mutat. Res. 486*, 217−247.
2. Niedernhofer, L. J., Riley, M., SchnetzBoutaud, N., Sanduwaran, G., Chaudhary, A. K., Reddy, G. R., and Marnett, L. J. (1997) Temperature-dependent formation of a conjugate between tris-(hydroxymethyl)aminomethane buffer and the malondialdehyde−DNA adduct pyrimidopurinone, *Chem. Res. Toxicol. 10*, 556−561.
3. Dong, Q., Johnson, S. P., Colvin, O. M., Bullock, N., Kilborn, C., Runyon, G., Sullivan, D. M., Easton, J., Bigner, D. D., Nahta, R., Marks, J., Modrich, P., and Friedman, H. S. (1999) Multiple DNA repair mechanisms and alkylator resistance in the human medulloblastoma cell line D-283 Med (4-HCR), *Cancer Chemother. Pharmacol. 43*, 73−79.
4. Mirikawa, K., Shirakawa, M. (2000) *Mutat. Res. 460*, 257−275.
5. Lage, C., de Padula, M., de Alencar, T. A. M., Goncalves, S. R. D., Vidal, L. D., Cabral-Neto, J., and Leitao, A. C. (2003) New insights on how nucleotide excision repair could remove DNA adducts induced by chemotherapeutic agents and psoralens plus UV-A (PUVA) in *Escherichia coli* cells, *Mutat. Res. 544*, 143−157.
6. Dronkert, M. L. G., and Kanaar, R. (2001) Repair of DNA interstrand cross-links, *Mutat. Res. 486*, 217−247.
7. Russmann, C., Stollhof, J., Weiss, C., Beigang, R., and Beato, M. (1998) Two wavelength femtosecond laser induced DNA−protein cross-linking, *Nucleic Acids Res. 26*, 3967−3970.
8. Cadet, J. V., P. (1990) *The Photochemistry of Nucleic Acids*, Wiley, New York.
9. Cleaver, J. E., and Crowley, E. (2002) UV damage, DNA repair, and skin carcinogenesis, *Front. Biosci. 7*, D1024−D1043.
10. Bredberg, A., Lambert, B., and Soderhall, S. (1982) Induction and repair of psoralen cross-links in DNA of normal human and xeroderma pigmentosum fibroblasts, *Mutat. Res. 93*, 221−234.
11. Tomic, M. T., Wemmer, D. E., and Kim, S. H. (1987) Structure of a psoralen cross-linked DNA in solution by nuclear magnetic resonance, *Science 238*, 1722−1725.
12. Eichman, B. F., Mooers, B. H. M., Alberti, M., Hearst, J. E., and Ho, P. S. (2001) The crystal structures of psoralen cross-linked DNAs: Drug-dependent formation of Holliday junctions, *J. Mol. Biol. 308*, 15−26.
13. Hwang, G. S., Kim, J. K., and Choi, B. S. (1996) The solution structure of a psoralen cross-linked DNA duplex by NMR and relaxation matrix refinement, *Biochem. Biophys. Res. Commun. 219*, 191−197.
14. Spielmann, H. P., Dwyer, T. J., Hearst, J. E., and Wemmer, D. E. (1995) Solution sStructures of psoralen monoadducted and cross-linked DNA oligomers by NMR spectroscopy and restrained molecular dynamics, *Biochemistry 34*, 12937−12953.
15. Kumaresan, K. R., Ramaswamy, M., and Yeung, A. T. (1992) Structure of the DNA interstrand cross-link of 4,5′,8-trimethylpsoralen, *Biochemistry 31*, 6774−6783.
16. Noll, D. M., Noronha, A. M., and Miller, P. S. (2001) Synthesis and characterization of DNA duplexes containing an N(4)C-ethyl-N(4)C interstrand cross-link, *J. Am. Chem. Soc. 123*, 3405−3411.
17. Noronha, A. M., Noll, D. M., and Miller, P. S. (2001) Syntheses of DNA duplexes containing a C−C interstrand cross-link, *Nucleosides Nucleotides Nucleic Acids 20*, 1303−1307.
18. Noronha, A. M., Noll, D. M., Wilds, C. J., and Miller, P. S. (2002) N(4)C-Ethyl-N(4)C cross-linked DNA: Synthesis and characterization of duplexes with interstrand cross-links of different orientations, *Biochemistry 41*, 760−771.
19. Noronha, A. M., Wilds, C. J., and Miller, P. S. (2002) N^{4}C-Alkyl-N^{4}C cross-linked DNA: Bending deformations in duplexes that contain a −CNG− interstrand cross-link, *Biochemistry 41*, 8605−8612.
20. Wilds, C. J., Noronha, A. M., Robidoux, S., and Miller, P. S. (2004) Mispair-aligned N3T-alkyl-N3T interstrand cross-linked DNA: Synthesis and characterization of duplexes with interstrand cross-links of variable lengths, *J. Am. Chem. Soc. 126*, 9257−9265.
21. Webba da Silva M, N. A., Noll, D. M., Miller, P. S., Colvin, O. M., and Gamcsik, M. P. (2002) Solution structure of a DNA duplex containing mispair-aligned N4C-ethyl-N4C interstrand cross-linked cytosines, *Biochemistry 41*, 15181−15188.
22. Jeener, J., Meier, B. H., Bachmann, P., and Ernst, R. R. (1979) Investigation of exchange processes by two-dimensional NMR spectroscopy, *J. Chem. Phys. 71*, 4546−4554.
23. Piantini, U., Sorensen, O. W., and Ernst, R. R. (1982) Multiple quantum filters for elucidating NMR coupling networks, *J. Am. Chem. Soc. 104*, 6800−6801.
24. Braunsweiler, L., and Ernst, R. R. (1987) Coherence transfer by isotropic mixing: Applications to proton correlation spectroscopy, *J. Magn. Reson. 53*, 521−528.
25. Gueron, M., and Plateau, P. (1982) Exchangeable proton NMR without base-line distortion, using new strong-pulse sequences, *J. Am. Chem. Soc. 104*, 7310−7311.
26. Piotto, M., Saudek, V., and Sklenar, V. (1992) Gradient-tailored excitation for single-quantum NMR spectroscopy of aqueous solutions, *J. Biomol. NMR 2*, 661−665.
27. Saenger, W. (1984) *Principles of Nucleic Acid Structure*, Springer-Verlag, Inc., New York.
28. Lavery, R., and Sklenar, H. (1989) Defining the structure of irregular nucleic acids: Conventions and principles, *J. Biomol. Struct. Dyn. 6*, 655−667.
29. Brunger, A. T. (1992) Department of Molecular Biophysics and Biochemistry, Yale University, New Haven, CT.
30. Brooks, B. R., Bruccoleri, R. E., Olafson, B. D., States, D. J., Swaminathan, S., and Karplus, M. (1983) CHARMM: A program for macromolecular energy minimization and dynamics calculations, *J. Comput. Chem. 4*, 187−217.
31. Clore, G. M., Gronenborn, A. M., Carlson, G., and Meyer, E. F. (1986) Stereochemistry of binding of the tetrapeptide acetyl-Pro-Ala-Pro-Tyr-NH_2 to porcine pancreatic elastase. Combined use of two-dimensional transferred nuclear Overhauser enhancement measurements, restrained molecular dynamics, X-ray crystallography, and molecular modelling, *J. Mol. Biol. 190*, 259−267.
32. Berendsen, H. J. C., Postma, J. P. M., Vangusteren, W. F., Dinola, A., and Haak, J. R. (1984) Molecular-dynamics with coupling to an external bath, *J. Chem. Phys. 81*, 3684−3690.
33. Ryckaert, J.-P., Ciccotti, G., and Berendsen, H. J. C. (1977) Numerical integration of the Cartesion equations of motion of a system with constraints: Molecular dynamics of *n*-alkanes, *J. Comput. Phys. 23*, 327−341.
34. Wijmenga, S. S., Mooren, M. M. W., and Hilbers, C. W. (1993) In *NMR of Macromolecules, A Practical Approach* (Roberts, G. C. K., Ed.) pp 217−288, Oxford University Press, New York.
35. Wuthrich, K. (1986) *NMR of Proteins and Nucleic Acids*, John Wiley and Sons, Inc., New York.
36. Hosur, R. V., Govil, G., and Miles, H. T. (1988) Application of two-dimensional NMR-spectroscopy in the determination of solution conformation of nucleic acids, *Magn. Reson. Chem. 26*, 927−944.
37. Thurston, D. E. (1999) Nucleic acid targeting: Therapeutic strategies for the 21st century, *Br. J. Cancer 80*, 65−85.
38. Gregson, S. J., Howard, P. W., Hartley, J. A., Brooks, N. A., Adams, L. J., Jenkins, T. C., Kelland, L. R., and Thurston, D. E. (2001) Design, synthesis, and evaluation of a novel pyrrolobenzodiazepine DNA-interactive agent with highly efficient cross-linking ability and potent cytotoxicity, *J. Med. Chem. 44*, 737−748.

BI0486435